Propagating fronts, chaos and multistability in a cell replication model

Rebecca Crabb
Department of Applied Mathematics, University of Washington, Seattle, Washington 98195

Michael C. Mackey
Center for Nonlinear Dynamics and Departments of Physiology, Physics, and Mathematics, McGill University, 3655 Drummond, Room 1124, Montreal, Quebec, H3G 1Y6, Canada

Alejandro D. Rey
Department of Chemical Engineering, McGill University, 3455 University Street, Montreal, Quebec, H3A 2A7, Canada

(Received 3 November 1995; accepted for publication 12 June 1996)

Numerical solutions to a model equation that describes cell population dynamics are presented and analyzed. A distinctive feature of the model equation (a hyperbolic partial differential equation) is the presence of delayed arguments in the time (t) and maturation (x) variables due to the nonzero length of the cell cycle. This transport like equation balances a linear convection with a nonlinear, nonlocal, and delayed reaction term. The linear convection term acts to impress the value of $u(t,x=0)$ on the entire population while the death term acts to drive the population to extinction. The rich phenomenology of solution behaviour presented here arises from the nonlinear, nonlocal birth term. The existence of this kinetic nonlinearity accounts for the existence and propagation of soliton-like or front solutions, while the increasing effect of nonlocality and temporal delays acts to produce a fine periodic structure on the trailing part of the front. This nonlinear, nonlocal, and delayed kinetic term is also shown to be responsible for the existence of a Hopf bifurcation and subsequent period doublings to apparent ''chaos'' along the characteristics of this hyperbolic partial differential equation. In the time maturation plane, the combined effects of nonlinearity, nonlocality, and delays leads to solution behaviour exhibiting spatial chaos for certain parameter values. Although analytic results are not available for the system we have studied, consistency and validation of the numerical results was achieved by using different numerical methods. A general conclusion of this work, of interest for the understanding of any biological system modeled by a hyperbolic delayed partial differential equation, is that increasing the spatio-temporal delays will often lead to spatial complexity and irregular wave propagation. [S1054-1500(96)00903-2]

When models of cell populations are built to account for biochemical processes and for the age distribution of cells, the resulting mathematical framework typically involves differential equations with inherent delays. In this work, the basic mechanisms involved in cell replication were accounted for in the derivation of a prototype delay equation model, which contains both temporal and spatial delays. The predictions of this model include soliton-like propagating fronts and spatio-temporal oscillations in cell densities, along with bifurcations and chaos. Increasing the spatiotemporal delays tends to lead to increased complexity.

I. INTRODUCTION

For cellular populations reproducing through binary fission (in contrast, e.g., to budding yeast), the dynamics are most naturally described in a modeling context by time-age-maturation models (see Ref. 1 for an excellent introduction). Often because of the nature of the boundary conditions, these partial differential equation models can be reduced to differential delay equation type models[2] or to delayed partial differential equation formulations.[3–7]

In this paper, the dynamics of a mathematical model for cell replication, in which there is simultaneous proliferation and maturation, is studied. The cell population dynamics are described by a first order nonlinear partial differential equation in which there is retardation in both the temporal and maturation variables. This model is novel because dynamical systems with retardation in both time and space have not been extensively studied. The resulting first order nonlinear partial differential equation for the cell density $u(t,x)$, in which there is retardation in both the temporal (t) and maturation (x) variables, is studied for the initial condition $\varphi(x)=x^n$. With this initial condition, varying the parameters of the model can lead to different types of dynamics ranging from a single stationary steady state to turbulent solution behaviour, and the eventual solution behaviour of the model also displays significant sensitivity to the initial function (multistability).

The model analyzed here is an extension of a previous model[8] that successfully accounted for some of the major clinical features of periodic hematopoiesis in humans and the experimental manifestations of this disorder in the gray collie.[2] As such, it offers the first steps toward the development of a tool with which to understand the effects of recombinant cytokines[9,10] on the dynamics of this disease, and with which one can explore the often confusing responses of the hematopoietic system to either chemotherapy, or bone mar-

row transplant preceded by whole body irradiation.[11,12]

The plan of the paper is as follows. In Section II, the motivation behind the model and its development are presented. In Section III we briefly summarize the numerical methods we have used to investigate the solution properties. In Section IV, we show through a sequence of illustrative numerical examples how traveling front solutions may arise, and that these solutions have soliton like properties. An understanding of these properties is given by results[13] on an analogous problem in the absence of retardation and nonlocality, and these are reviewed in the first part of Section IV. In Section V we turn to a consideration of the multi-stable behaviour of the eventual solutions. We first review previous work on this problem,[4–7] and then present a number of new numerical results on the dynamics of the temporal and spatial solutions that indicate the complexity of the multistability and bifurcation structure of this interesting and novel system. The paper concludes with a brief discussion in Section VI.

II. DEVELOPMENT OF THE BIOLOGICAL MODEL

A cell produces two daughter cells by going through two phases, an interphase and a division phase. Since each daughter cell must contain the same components as its parent cell, in order for a cell to divide it must duplicate all of its contents. This occurs during the interphase. The interphase is divided into three phases G_1, S, and G_2. During the G_1 phase, the cell increases its rate of biosynthesis before entering the S phase during which the cell synthesizes its DNA and duplicates the contents of its nucleus. The cell then goes through the G_2 phase before entering the division phase or M phase and dividing via mitosis and cytokinesis.[14]

Cells are considered to be actively proliferating if they are in the $G1/S/G2/M$ cycle and if they are committed to replicating their DNA and continuing through mitosis and cytokinesis to produce two daughter cells. Let a denote the cell age, i.e., the position of the cell in the cell cycle, with a ranging from $a=0$, at the point of commitment, to $a=\tau$, at the point of cytokinesis. Some authors have examined the role of distributions of ages in time age models, notably Refs. 15–21, and obtained results that can be applied to some types of cell cycle models. Their results indicate, at least in a model without the maturation dimension, significant new effects are not to be expected to arise from a distribution of cell cycle times and we have not considered it here, though it is the subject of active investigation in our group.

As well as proliferating, cells can also be characterized by other processes such as maturation. The level of maturation is measured in different ways for different cells. In keeping with experimental evidence,[22,23] we assume that the aging and maturation processes take place simultaneously and independently. Let x represent the maturation variable. If the maturation variable runs from a minimal value of $x_{\min}$ to a finite maximal value of $x_{\max}$, then we may rescale x and replace it with a new x given by $(x-x_{\min})/(x_{\max}-x_{\min})$ so the scaled maturation variable runs from 0 to 1. Thus, the range of the values of x is taken from $x=0$ to $x=1$ without loss of generality. Since cells can mature at different rates depending on their maturation x we assume that it is linear and a maturation rate r is introduced so the velocity of maturation is $V(x)=rx$ for $x \in (0,1)$ and $V(0)=0$ and $V(1)=r$.

We further assume that a cell can disappear through death at any time during its life, and we let γ denote the rate at which cells die. γ is positive and assumed to be independent of the age or the maturation level of the cell.

It should be noted that a number of authors have employed time-age or time-maturation models for the description of cell replication processes, but the terminology is by no means consistent. For example, in Refs. 24–26 models are discussed in which age denotes the time since the birth of a cell—just as we do. In Ref. 27, however, the term maturation is used for this quantity. Given the quite explicit definitions of the terms age and maturation as used here, the reader should have no difficulty in discerning the differences.

We now turn to a derivation of the equations governing this process. The derivation could have been carried out along the lines of that in Ref. 3, but here we present a somewhat abbreviated and *ad hoc* derivation. The reader interested in the full details should consult Ref. 3.

Let $U(t,x,a)$ denote the density of proliferating cells, where x and a are as described above and t is time. Then

$$\frac{\partial U}{\partial t}+\frac{\partial U}{\partial a}+\frac{\partial [rxU]}{\partial x}=-\gamma U \tag{1}$$

is the conservation equation for $U(t,x,a)$ with initial condition

$$U(0,x,a)=\Gamma(x,a), \quad \text{for } (x,a)\in[0,1]\times[0,\tau]. \tag{2}$$

The total number of proliferating cells is given by

$$u(t,x)=\int_0^\tau U(t,x,a)\,da, \tag{3}$$

and the boundary conditions for the system are

$$U(t,x,0)=2U(t,x,\tau)=\mathcal{F}(u(t,x)). \tag{4}$$

The first equality reflects the fact that two daughter cells generated at $a=\tau$, i.e. at the end of the cycle, constitute the input flux for the cell cycle at $a=0$. The second equality states that the input flux $\mathcal{F}$ is assumed to be a function of the total number of proliferating cells at a given maturation level. Equation (1) can be rewritten as

$$\frac{\partial U}{\partial t}+\frac{\partial U}{\partial a}+rx\frac{\partial U}{\partial x}=-[\gamma+r]U. \tag{5}$$

The general solution of (5) can be calculated using the method of characteristics.[28] The characteristic equations are

$$\frac{\partial t}{\partial s}=1, \quad \frac{\partial a}{\partial s}=1, \quad \frac{\partial x}{\partial s}=rx, \quad \text{and } \frac{\partial U}{\partial s}=-[\gamma+r]U, \tag{6}$$

which, after integration, give the set of parametric equations

$$\begin{aligned} &t(s)=s+t_0, \quad a(s)=s+a_0,\\ &x(s)=x_0e^{rs}, \quad U(s)=U_0e^{-[\gamma+r]s}. \end{aligned} \tag{7}$$

To obtain an explicit solution, two cases are considered: $0 \leqslant t \leqslant a$ and $a < t$. For $0 \leqslant t \leqslant a$, the initial condition $U(0,x,a) = \Gamma(x,a)$ is used. Thus, $t = s = 0$ on the initial curve and

$$t = s, \quad a = t + a_0, \quad x = x_0 e^{rt}, \quad U = U_0 e^{-[\gamma + r]t}, \tag{8}$$

which gives

$$U(t,x,a) = \Gamma(xe^{-rt}, a - t)e^{-[\gamma + r]t}, \quad 0 \leqslant t \leqslant a. \tag{9}$$

For $a < t$, $U(t,x,a) = U(t,x,0)$. Thus, $a = s = 0$ on the initial curve and

$$t = a + t_0, \quad a = s, \quad x = x_0 e^{ra}, \quad U = U_0 e^{-[\gamma + r]a}, \tag{10}$$

which gives

$$U(t,x,a) = U(t - a, xe^{-ra}, 0)e^{-[\gamma + r]a}, \quad a < t. \tag{11}$$

Hence,

$$U(t,x,a) = \begin{cases} \Gamma(xe^{-rt}, a - t)e^{-[\gamma + r]t}, & 0 \leqslant t \leqslant a, \\ U(t - a, xe^{-ra}, 0)e^{-[\gamma + r]a}, & a < t. \end{cases} \tag{12}$$

Equation (5) can be integrated over the age variable a which, in conjunction with (3), gives

$$\frac{\partial u}{\partial t} + rx\frac{\partial u}{\partial x} = -[\gamma + r]u - \{U(t,x,\tau) - U(t,x,0)\}. \tag{13}$$

After applying the boundary conditions (4) and using the general solution (12), equation (13) becomes

$$\frac{\partial u}{\partial t} + rx\frac{\partial u}{\partial x} = -[\gamma + r]u + \begin{cases} \Gamma(xe^{-rt}, \tau - t)e^{-[\gamma + r]t}, & 0 \leqslant t \leqslant \tau, \\ \mathscr{F}(u(t - \tau, xe^{-r\tau}))e^{-[\gamma + r]\tau}, & \tau < t. \end{cases} \tag{14}$$

The interesting case to study is when $\tau < t$, i.e. when

$$\frac{\partial u}{\partial t} + rx\frac{\partial u}{\partial x} = -[\gamma + r]u + \mathscr{F}(u(t - \tau, xe^{-r\tau}))e^{-[\gamma + r]\tau}, \tag{15}$$

since we are interested in the long time behaviour of the solution. As described above, the input flux $\mathscr{F}$ is a function of the total number of proliferating cells at a given maturation level.

Realizing that the input flux $\mathscr{F}$ is given by the product of the proliferation rate and the cell density u, and taking the proliferation rate to be a linearly decreasing function of u given by $2c(1-u)$, we have

$$\mathscr{F}(u) = 2cu(1 - u). \tag{16}$$

[Note that it would be more realistic biologically to take a non-negative monotone decreasing function for the proliferation rate such as

$$2c\frac{\theta^m}{\theta^m + u^m}, \quad \theta, m > 0. \tag{17}$$

However, we have chosen the linearly decreasing proliferation rate to facilitate the analytic computation of the solution to (15) in the case that $\tau = 0$.]

If we also set

$$\delta = \gamma + r \quad \text{and} \quad \lambda = ce^{-(\gamma + r)\tau}, \tag{18}$$

then (15) becomes

$$\frac{\partial u}{\partial t} + rx\frac{\partial u}{\partial x} = -\delta u + \lambda u_\tau(1 - u_\tau), \tag{19}$$

where u_τ is defined by

$$u_\tau(t,x) \equiv u(t - \tau, xe^{-r\tau}). \tag{20}$$

Both the nonlocality ($xe^{-r\tau}$) and the temporal ($t - \tau$) retardation, which are the essential novel ingredients of (15), are clearly represented in (19). These two features make the study of (15) extremely interesting. The study of systems with both nonlocality and temporal retardation has been partially explored by Rey and Mackey.[4–7]

Throughout this paper, we employ the initial condition

$$IC: u(t - \tau, xe^{-r\tau}) = \varphi(x) = x^n, \quad 0 \leqslant t \leqslant \tau, \quad n \geqslant 1, \tag{21}$$

and the boundary condition

$$BC: u(t, x = 0) = 0, \quad t \in \Re^+. \tag{22}$$

We were motivated to study this specific form of initial condition because it allows us to explore the possible consequences of widespread destruction of proliferating cells, as would be encountered, for example, after chemotherapy and/or radiotherapy. As in the experimental/clinical situation this initial condition makes the destruction an inverse function of cell maturation.

III. NUMERICAL METHODS OF SOLUTION

The numerical methods used to integrate the partial differential delay equation are the Galerkin finite elements method[29–31] and the method of characteristics,[28] and in this section we briefly review both.

A. The Galerkin finite elements method (GFEM)

The GFEM assumes that given a nonlinear partial differential equation such as (19), $u(t,x)$ can be accurately represented by an approximate solution $u_a(t,x)$ of the form

$$u_a(t,x) = \sum_{j=1}^{N} u_j(t)\varphi_j(x), \tag{23}$$

where the u_j are unknown coefficients, the φ_j are known basis functions, and N is the number of nodes in the discretization of the maturation variable. Substituting u_a into the nonlinear partial differential equation (19), the nonzero residual R is obtained:

$$R = \frac{\partial u_a}{\partial t} + rx\frac{\partial u_a}{\partial x} + \delta u_a - \lambda u_{a_\tau}(1 - u_{a_\tau}). \tag{24}$$

R cannot be null since u_a is an approximate solution. Hence R is forced to zero, which gives the weighted residual:

$$F_i = \int_0^1 \left[\frac{\partial u_a}{\partial t} + rx \frac{\partial u_a}{\partial x} + \delta u_a - \lambda u_{a_\tau}(1-u_{a_\tau}) \right] \varphi_i dx, \quad i = 1, \ldots, N, \tag{25}$$

where φ_i are the same basis functions as in (23).

A time discretization of $(\partial u_a/\partial t)$ is then implemented using a finite difference scheme and the resulting set of nonlinear algebraic equations can be solved using an iterative root finder such as the Newton–Raphson scheme.[29–31] The code implementing the GFEM is written in FORTRAN. Linear basis and weighting functions are used as well as a uniform mesh of 400–600 elements ($N=401-601$). The time integration scheme is a first order implicit predictor corrector method with fixed time step. With no delay the time step is $h=1/50$, and with delay the time step is $h=\tau/50$.

B. The method of characteristics

The method of characteristics is applicable to quasilinear partial differential equations. The main idea behind the method of characteristics is to transform the delayed partial differential equation into an ordinary delayed differential equation which one can then solve using the initial condition(s).[28]

The x characteristics of (19) are given by $x(t)=x_0 e^{rt}$. Along these characteristics, (19) is rewritten as

$$\frac{du}{dt} = -\delta u + \lambda u_\tau (1-u_\tau), \tag{26}$$

where

$$u(t,x(t)) \equiv u(t,x_0 e^{rt}) \tag{27}$$

and

$$u_\tau(t,x(t)) \equiv u(t-\tau, x_0 e^{r(t-\tau)}). \tag{28}$$

The code for the integration along characteristics is written in C. A fourth order Runge–Kutta method is used with a constant time step of 10^{-5}.

IV. PROPAGATING FRONT SOLUTIONS

In this section we numerically explore the nature of propagating front solutions to (15). There has been considerable work[13,32–38] characterizing the nature of the solutions to (15) in the absence of a delay ($\tau=0$) and thus the absence of nonlocality, and we first review the major results of importance.

A. Results for $\tau=0$

There are several interesting results concerning the solution behaviour of first order partial differential equations with respect to stability and exactness (see above references), and most of this work was initiated by the work of Lasota[13] who considers the partial differential equation

$$\frac{\partial u}{\partial t} + c(t,x)\frac{\partial u}{\partial x} = f(t,x,u), \quad (t,x) \in [0,\infty] \times [0,1], \tag{29}$$

with the initial condition

$$u(0,x) = \varphi(x), \quad \text{for } x \in [0,1]. \tag{30}$$

In this section we discuss those results as they relate to the unretarded ($\tau=0$) version of (19).

The results of Lasota[13] are directly applicable to the system studied here with no delay ($\tau=0$) and given by

$$\frac{\partial u}{\partial t} + rx\frac{\partial u}{\partial x} = -\delta u + \lambda u(1-u), \tag{31}$$

where

$$\delta = \gamma + r \quad \text{and} \quad \lambda = c, \tag{32}$$

and the initial and boundary conditions are

$$IC: \varphi(x) = u(0,x) = x^n m, \quad x \in [0,1], \tag{33}$$

$$BC: u(t, x=0) = 0 \quad t \in \Re^+. \tag{34}$$

An analytic solution of (31) can be obtained using the method of characteristics, and is of some help in illuminating the numerical behaviour discussed in the following section when $\tau>0$. This solution is

$$u(t,x) = \frac{[(\lambda-\delta)/\lambda](xe^{-rt})^n e^{t(\lambda-\delta)}}{(xe^{-rt})^n (e^{t(\lambda-\delta)}-1) + [(\lambda-\delta)/\lambda]}. \tag{35}$$

The limiting behaviour of the analytic solution (35) is as follows [remember the condition (34)]:

$$\lim_{t\to\infty} u(t,x) = \begin{cases} 0, & 0 < \lambda - \delta < nr, \\ \dfrac{(\lambda-\delta)x^n}{\lambda - \delta + \lambda x^n}, & \lambda - \delta = nr, \\ \dfrac{\lambda-\delta}{\lambda}, & \lambda - \delta > nr. \end{cases} \tag{36}$$

The solution behaviour obtained for $nr<\lambda-\delta$, when n is taken to be sufficiently large, is that of moving fronts. Front solutions, as defined by Collet and Eckman,[39] ''interpolate between two (different) stationary solutions at $x=\pm\infty$; in addition, they move with a certain speed in the laboratory frame.'' Here, this definition is slightly modified. Since x is only considered in the interval $[0,1]$, the front solution interpolates between two stationary solutions, namely the trivial solution, at $x=0$, and the solution $(\lambda-\delta)/\lambda$, at $x=1$, and the front speed is thus time dependent.

The solution behaviour of moving fronts for $nr<\lambda-\delta$ can be summarized as follows: increasing either n or r slows down the rate at which the solution approaches its limiting behaviour, and hence reduces the speed at which the front propagates towards the impermeable boundary at $x=0$. The former effect is due to the fact that increasing n produces a steeper initial profile, while the latter effect arises because increasing r increases the strength of the convective term $(r\partial u/\partial x)$ which, in turn, opposes front propagation.

B. New results for $\tau>0$

There is no known method to obtain an analytic solution of (19) with $\tau>0$. Hence the results of this section are nu-

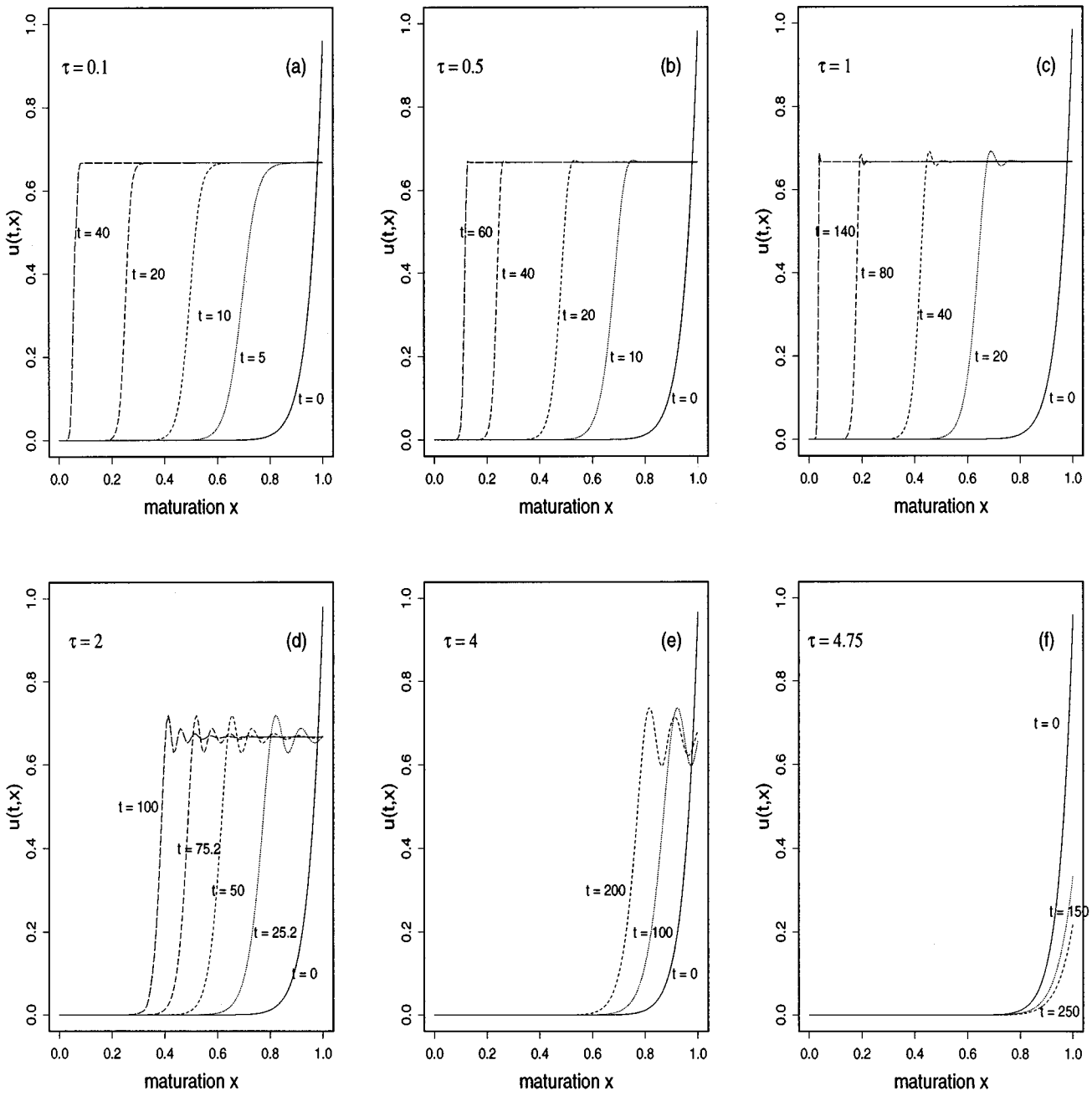

FIG. 1. Effect of increasing τ on the solution behaviour for $n=20$, $r=0.01$, $\delta=1$, and $\lambda=3$.

merical solutions to (19) subject to conditions (21) and (22). The accuracy of these results was checked in three ways.

(1) The numerical solutions obtained with $\tau=0$ were compared to the analytic solution (35).
(2) In the GFEM, the number of elements were doubled and quadrupled to check for changes in the solution behaviour.
(3) The solutions obtained with the GFEM were compared to those obtained numerically using the method of characteristics for $\tau>0$.

The results obtained from all of these checks indicate that the GFEM code is correct in the sense that the numerically determined solutions match the analytic ones, and, when analytic solutions are not available, it produces mesh independent solutions that agree with those obtained using the method of characteristics. Throughout this section we take $\delta=1$, $\lambda=3$, $r=0.01$, and $n=20$, and examine the effect of τ on the solution behaviour.

1. Effect of increasing τ

The effect of increasing τ is illustrated in Fig. 1. When τ is close to 0, it can be shown that the solution is similar to the solution for $\tau=0$, i.e. the solution for small x starts at the trivial solution, and as x increases towards 1, smoothly ap-

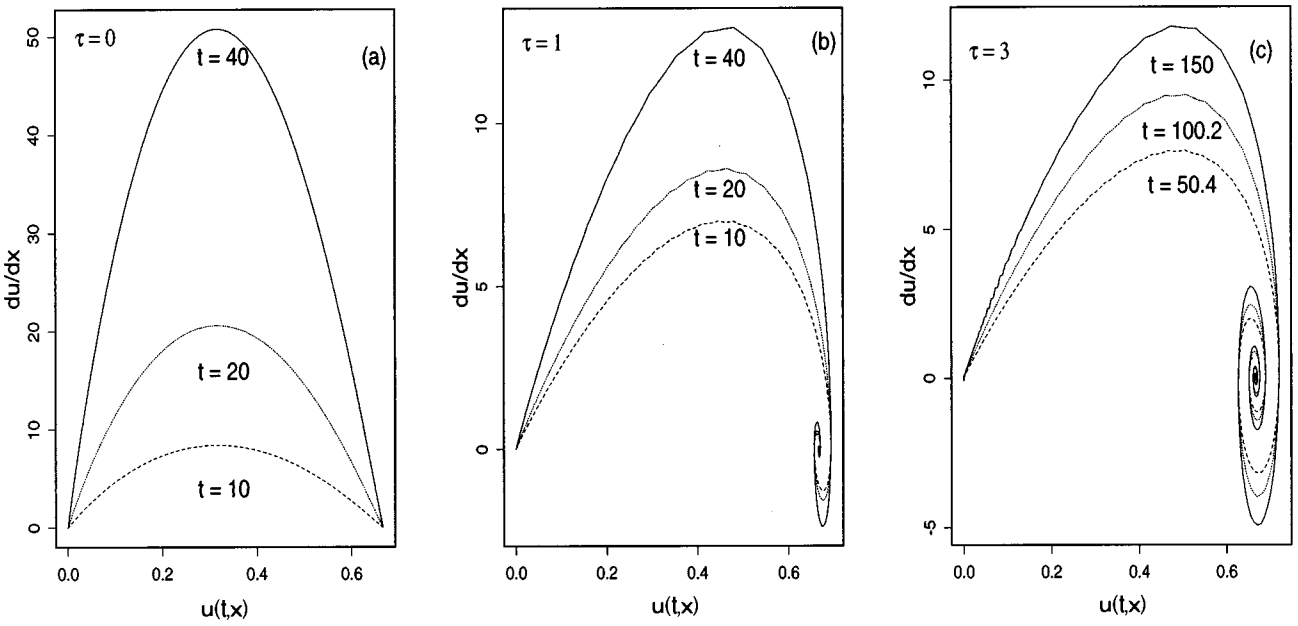

FIG. 2. Phase-plane diagrams of the solution behaviour for various values of τ with $n=20$, $r=0.01$, $\delta=1$, and $\lambda=3$.

proaches the $(\lambda-\delta)/\lambda$ solution. However, as τ is increased the speed at which the front moves towards the impermeable boundary $x=0$ decreases until the front completely disappears for a critical value of $\tau=\tau_c$. At $\tau=\tau_c$ the solution is no longer attracted to the $(\lambda-\delta)/\lambda$ solution. This bifurcation in solution behaviour appears between $\tau=4$ and $\tau=4.75$, and is due to the fact that the long time behaviour switches from the $(\lambda-\delta)/\lambda$ solution, for $\tau<\tau_c$ to the trivial solution when $\tau>\tau_c$. This switch is similar to the one Lasota[13] demonstrated analytically for $\tau=0$ [cf. equation (36)], though much more complex than in the simple case of $\tau=0$.

Another change in the solution behaviour occurs as τ is increased from 0 to τ_c. Although the solution still starts out at the trivial solution for small x, as x increases, instead of making the transition smoothly to the $(\lambda-\delta)/\lambda$ solution, the solution approaches $(\lambda-\delta)/\lambda$ in an oscillatory fashion. The amplitude of these oscillations increases as τ increases. This is clearly observed, in Figure 1, by the change in solution behaviour between $\tau=0.1$ and $\tau=4$.

2. An oscillating solution around $(\lambda-\delta)/\lambda$

In Figure 1, it was observed that oscillations appeared with a small visible peak for $\tau=0.5$ and that as τ was increased the amplitude of the oscillations became larger. The amplitude of the oscillations, observed in Figure 1d, decreases as x increases; these oscillations are therefore damped oscillations. Further, it can be shown that as τ is increased the wave length increases. Hence, the results shown in Figure 1d indicate that the oscillations in the solution behaviour are damped with increasing wave length as τ is increased.

To obtain further insight into these phenomena, the (u,u_x) phase-plane diagrams of the solution behaviour are shown in Figure 2 where $\partial u(t,x)/\partial x$ is plotted versus $u(t,x)$. The phase-plane diagram for $\tau=0$ was obtained using the analytic solution (35):

$$\frac{du}{dx}=\frac{[(\lambda-\delta)/\lambda]^2(xe^{-rt})^n n e^{t(\lambda-\delta)}}{[(xe^{-rt})^n(e^{t(\lambda-\delta)}-1)+[(\lambda-\delta)/\lambda]]^2 x}. \tag{37}$$

The phase diagrams for $\tau>0$ were obtained using a difference scheme, and are not completely smooth because of computational limitations.

In the phase diagrams, the increase in the steepness of the front is shown by the increase in the values of du/dx. For instance, comparing the phase diagrams in Figure 2 for $\tau=0$ (Figure 2a) and $\tau=1$ (Figure 2b), one can see that the change in steepness of the front is not as great between times $t=10$ and $t=20$. This is due to the fact that the speed of propagation of the front is slower for $\tau=1$ than for $\tau=0$. Further, the appearance of the oscillations is reflected in the spiraling around the point $(\lambda-\delta)/\lambda$. The differences in the spirals for $\tau=1$ (Figure 2b) and for $\tau=3$ (Figure 2c) illustrate that, as τ is increased, the amplitude and the wave length of the oscillations become greater.

C. Section summary

The numerical study of (19), with the initial condition (21) and boundary condition (22) shows interesting solution behaviour for $n\gg 1$. As we have shown in Section IV A, the analytic solution with $\tau=0$ is a propagating wave front. The parameters n and r vary the speed at which the front propagates and can also lead to a change in stability. The numerical solution with $\tau>0$ is also a propagating front. However as the delay is increased, oscillations appear near the wave front. This type of solution can be associated with soliton-like behaviour. Although the changes from a monotone front to an oscillatory front in a delayed partial differential equation reported here appear to be new, this type of behaviour

has been observed in the solution of the KdV Burger's equation.[40] As the delay is increased past a critical delay τ_c, there is a change in stability, and the long term behaviour becomes that of the trivial solution.

From a biological perspective these numerical results indicate that following a massive depletion of cells, the cellular population will reconstitute itself with a speed that decreases as the cell cycle time τ increases. This repopulation may be either uniform, or oscillatory, but once the cell cycle time τ exceeds a critical threshold value of τ_c repopulation is impossible and the entire cellular population is driven to extinction.

V. MULTISTABLE SOLUTION BEHAVIOUR

In this section we turn from an examination of the propagating front solutions of Section IV to a consideration of the dependence of the eventual solution behaviour on the initial function. Throughout, we will take $n=1$ in the initial function equation (21).

A. Previous results

Rey and Mackey[3,4] studied the dynamics of the model (19) for two initial conditions $\varphi(x)=x+c$ and $\varphi(x)=x$. In this section, their results for $\varphi(x)=x$ are briefly summarized.

For $n=1$, the long time behaviour of (19) with $\tau=0$ and $0<\delta<\lambda$ with $\varphi(x)=x$ is

$$\lim_{t\to\infty} u(t,x)=\begin{cases} 0, & 0<\lambda-\delta<r, \\ \dfrac{(\lambda-\delta)x}{\lambda-\delta+\lambda x}, & \lambda-\delta=r, \\ \dfrac{\lambda-\delta}{\lambda}, & \lambda-\delta>r. \end{cases} \tag{38}$$

To extend these results to the case of $\tau>0$, the model (19) can be rewritten, using the method of characteristics, as

$$\frac{du}{dt}=-\delta u+\lambda u_\tau(1-u_\tau), \tag{39}$$

where

$$u(t,x(t))\equiv u(t,x_0e^{rt}) \tag{40}$$

and

$$u_\tau(t,x(t))\equiv u(t-\tau,x_0e^{r(t-\tau)}). \tag{41}$$

Using this method it is possible to determine the local temporal and spatial stability of the steady states separately.

Letting $\tau=1$ and linearizing (39) around the trivial solution, Rey and Mackey showed that there is an $r\equiv r_c$ which determines the local stability of the three solutions when subjected to linear spatial perturbations. For $r>r_c$, the trivial solution is locally stable and the two other solutions are locally unstable. When $r<r_c$ the $(\lambda-\delta)/\lambda$ solution is locally stable while the other two are locally unstable. Finally, for $r\equiv r_c$, the only solution which is locally stable is a nonhomogeneous one which we denote by $u_{nh}(x)$ throughout. This nonhomogeneous solution is locally stable when $\lambda=(\delta+r)e^r$.

Linearizing (39) around the nontrivial steady state $(\lambda-\delta)/\lambda$ gives the equation

$$\frac{dz}{dt}=-\delta z+(2\delta-\lambda)z_\tau, \tag{42}$$

where $z=u-[(\lambda-\delta)/\lambda]$. Under the assumption that the solutions to the linear equation (42) are of the form $z(t)\simeq e^{\kappa t}$ we obtain the eigenvalue equation

$$\kappa=-\delta+(2\delta-\lambda)e^{-\kappa}. \tag{43}$$

Since a transition from a single steady state to a periodic cycle is expected, we take

$$\kappa=\mu+i\omega, \tag{44}$$

which then gives

$$\mu+i\omega=-\delta+(2\delta-\lambda)e^{-\mu}e^{-iw}. \tag{45}$$

Separating real and imaginary parts, this last result can be written as

$$\begin{aligned} \mu&=-\delta+(2\delta-\lambda)e^{-\mu}\cos\omega, \\ \omega&=-(2\delta-\lambda)e^{-\mu}\sin\omega. \end{aligned} \tag{46}$$

Thus from the results of Hale,[41] the nontrivial steady state $(\lambda-\delta)/\lambda$ is locally stable $[\mu=\mathrm{Re}\,\lambda<0]$ if and only if

$$\sqrt{(2\delta-\lambda)^2-\delta^2}<\cos^{-1}\left(\frac{\delta}{2\delta-\lambda}\right), \tag{47}$$

and thus locally unstable when the inequality is reversed.

The equality

$$\sqrt{(2\delta-\lambda)^2-\delta^2}=\cos^{-1}\left(\frac{\delta}{2\delta-\lambda}\right) \tag{48}$$

defines a bifurcation point marking the transition from a single locally stable solution to a locally stable periodic cycle, and there are three possible spatial Hopf bifurcations depending on the relationship between the line composed of the (λ,δ) values satisfying this temporal Hopf bifurcation (denote this line by THB), and the line composed of the (λ,δ) values satisfying $\lambda=(\delta+r)e^r$ for which the $u_{nh}(x)$ solution is stable. Denote this latter line by SS.

If the line THB is always above the line SS (this occurs for $0<r<0.7455$) there is a simultaneous spatial and temporal Hopf bifurcation occurring when the $(\lambda-\delta)/\lambda$ solution loses its stability. The temporal bifurcation leads to periodic solution behaviour while the spatial bifurcation leads to left traveling waves. However, if the line SS crosses the line THB (this occurs when $0.7455<r<1.0986$) there is a spatial Hopf bifurcation occurring when the $u_{nh}(x)$ solution loses its stability. This Hopf bifurcation induces slow left traveling waves. Finally, if the line SS is always above the line THB (this occurs when $r>1.0986$) there is a spatial Hopf bifurcation also occurring when the $u_{nh}(x)$ solution loses its stability. In this situation the Hopf bifurcation leads to chaotic traveling waves. These results are summarized in Figure 3.

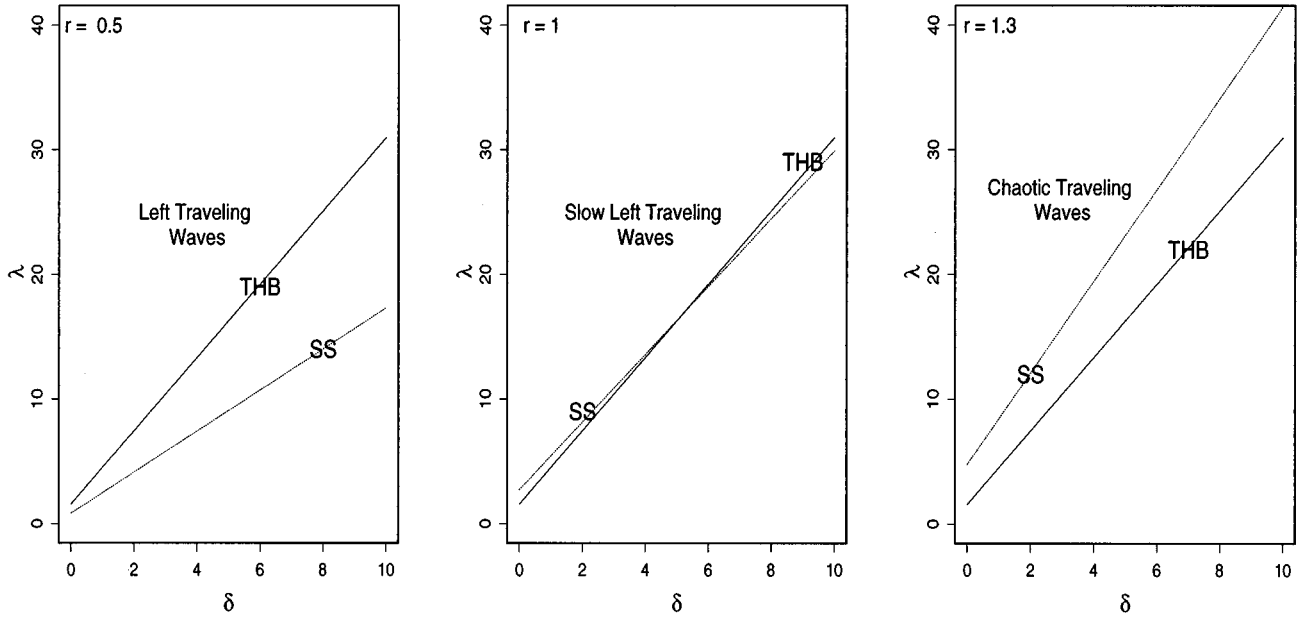

FIG. 3. Diagram of the three possible scenarios for which spatial Hopf bifurcations occur.

B. New results

In this section the case where $r \ll 0.7455$ is considered. For these values of r, a simultaneous temporal and spatial Hopf bifurcation occurs when

$$\sqrt{(2\delta-\lambda)^2-\delta^2} = \cos^{-1}\left(\frac{\delta}{2\delta-\lambda}\right) \tag{49}$$

is satisfied. The changes in solution behaviour of (19) subject to conditions (21) and (22) will be studied as the parameter λ is increased. With reference to Figure 3, the λ value always lies above the THB curve.

1. Temporal bifurcations occurring after the Hopf bifurcation

The bifurcation diagram for (19) is shown in Figure 4. This bifurcation diagram is obtained by calculating the solution along the characteristics given by (39) and plotting the local extrema of the solution $u(t,x)$ as a function of λ (the λ's are incremented by 10^{-5}) for $700<t<750$. In all cases δ, x_0, and r are held constant with the following values $\delta=1$, $x_0=0.1$, and $r=0.01$. The Hopf bifurcation occurs at $\lambda\simeq 4.25$ which concurs with the analytic results given by the local stability analysis [cf. equation (49)]. A period doubling bifurcation occurs at $\lambda\simeq 5.412$. At $\lambda\simeq 5.793$ there is a jump in the solution and a new cycle of period 8 occurs. As λ is increased past 5.793 the cycle of period 8 gives rise to a turbulent solution which appears to be chaotic. This turbulent solution ends abruptly at $\lambda\simeq 5.854$ at which point a new cycle of period 2 occurs.

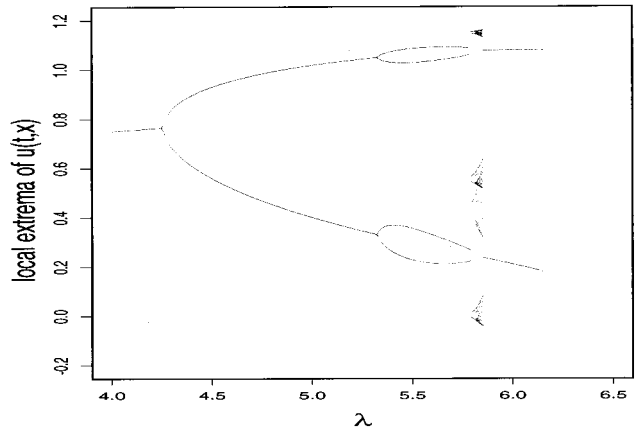

FIG. 4. Temporal bifurcation diagram for the model obtained by numerically computing the solution along the x characteristics given by (39) and plotting the local extrema of $u(t,x)$ versus λ.

To better visualize what is happening in the region from the first bifurcation (from a period 4 cycle to a period 8 cycle) to the second bifurcation (from a turbulent solution to a period 2 cycle), the bifurcation diagram of Figure 4 is magnified for $5.79<\lambda<5.87$, and shown in Figure 5.

Figure 5b shows a period doubling route to chaos. As λ is increased, the period doublings occur at smaller intervals of λ until the period doublings are no longer distinguishable and the solution becomes chaotic at $\lambda\simeq 5.8194$. Figures 5b–5c show that there are periodic windows in the chaotic attractor.

Subduction is a term given by Grebogi *et al.*[42] to describe the appearance of a nonchaotic attractor within a chaotic attractor causing the chaotic attractor to be replaced by the nonchaotic attractor. It would appear that these windows arise in Figure 5 by the appearance of periodic cycles in the chaotic attractor which destroy the chaotic attractor via subduction.

The chaotic attractor reappears through new period doubling routes to chaos and then widens. This widening is probably caused by the intersection of a locally unstable

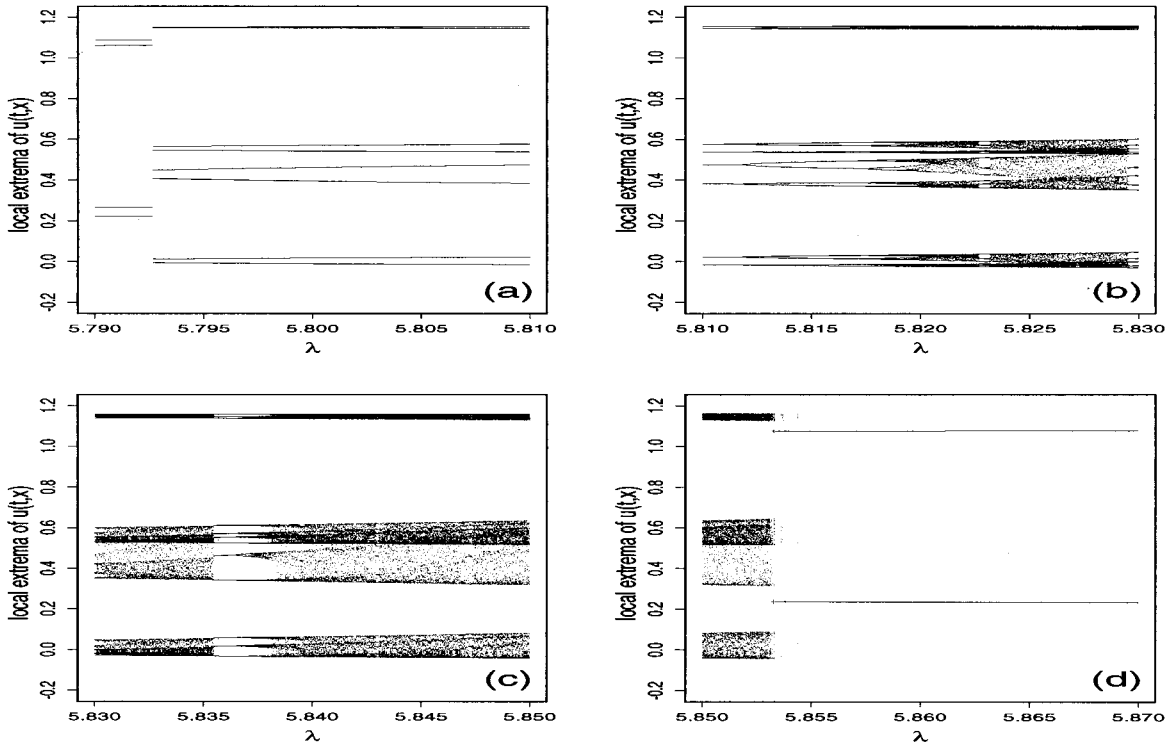

FIG. 5. Magnification of the bifurcation diagram in Figure 4 for $5.79<\lambda<5.87$.

cycle and the distinct chaotic bands; this phenomenon has been called an interior crisis.[42] The largest window occurs when $5.8356<\lambda<5.8372$. The cycle is of period 12 in this window.

In Figure 5d the chaotic attractor suddenly disappears and a new cycle of period 2 appears. By a conjecture of Grebogi *et al.*,[42] the destruction of this chaotic attractor is most probably caused by the collision of an unstable orbit with the chaotic attractor. It is not possible to determine from the numerical evidence of Figure 5d where the unstable orbit which causes the destruction is located.

2. Multistability of the solution along the x characteristics

The sudden jump from a period 4 cycle to a period 8 cycle as shown in Figure 5a is an indication that there are two coexisting attractors of the solution. Each attractor must have a basin of attraction such that given an initial condition in the basin of attraction the solution converges to the attractor as $t\to\infty$.

There has been an extensive study of the geometry of basins of attraction and of their boundaries in nonlinear return maps obtained from ordinary differential equations.[43–45] These basins of attraction can be extremely complicated, and in some cases are fractal in nature. Sensitivity to initial conditions has previously been studied for differential delay equations, and it has been shown that they can possess multistable solutions.[46–54] To determine whether the model (19) has two coexisting attractors the solutions obtained along the x characteristic at $\lambda=5.79$ and at $\lambda=5.81$ are taken as initial conditions. (Recall that at $\lambda=5.79$ the solution consists of a cycle of period 4 and at $\lambda=5.81$ the solution consists of a cycle of period 8; cf. Figure 4.)

The bifurcation diagram for the solution with an initial condition which is the solution at $\lambda=5.79$ is shown in Figure 6a. For comparison, in Figure 6b, the solution bifurcation diagram of Figure 4 is magnified for $5.7<\lambda<5.9$. The jump to a period 8 cycle as well as the subsequent period doublings and chaotic bands have completely disappeared (compare with Figure 6b) and instead there is a smooth transition from the cycle of period 4 to the cycle of period 2 at $\lambda\simeq5.82$. Call the attractor shown in Figure 6a attractor A. Comparing Figure 6a and Figure 6b, one sees that attractor A becomes unstable in Figure 6b for $5.793<\lambda<5.854$.

The bifurcation diagram for the solution when the initial condition is the solution at $\lambda=5.81$, is shown in Figure 7a. In Figure 7b, the bifurcation diagram in Figure 4 is again magnified for $5.7<\lambda<5.9$.

From Figure 7a, we see that instead of a solution bifurcation at $\lambda\simeq5.793$ from a period 4 cycle to a period 8 cycle, there is now a bifurcation from a period 4 cycle to a new period 4 cycle at $\lambda\simeq5.732$. The new period 4 cycle then gives rise to the period 8 cycle at $\lambda\simeq5.788$. The period doubling route to chaos as well as the periodic windows and the destruction of the chaotic attractor occur as before. Call the attractor shown in Figure 7a attractor B. Comparing Figure 7a and Figure 7b, one sees that attractor B is unstable in Figure 7b for $5.732<\lambda<5.793$.

One can very precisely determine the range of values of λ, for which the initial conditions (which are given by the

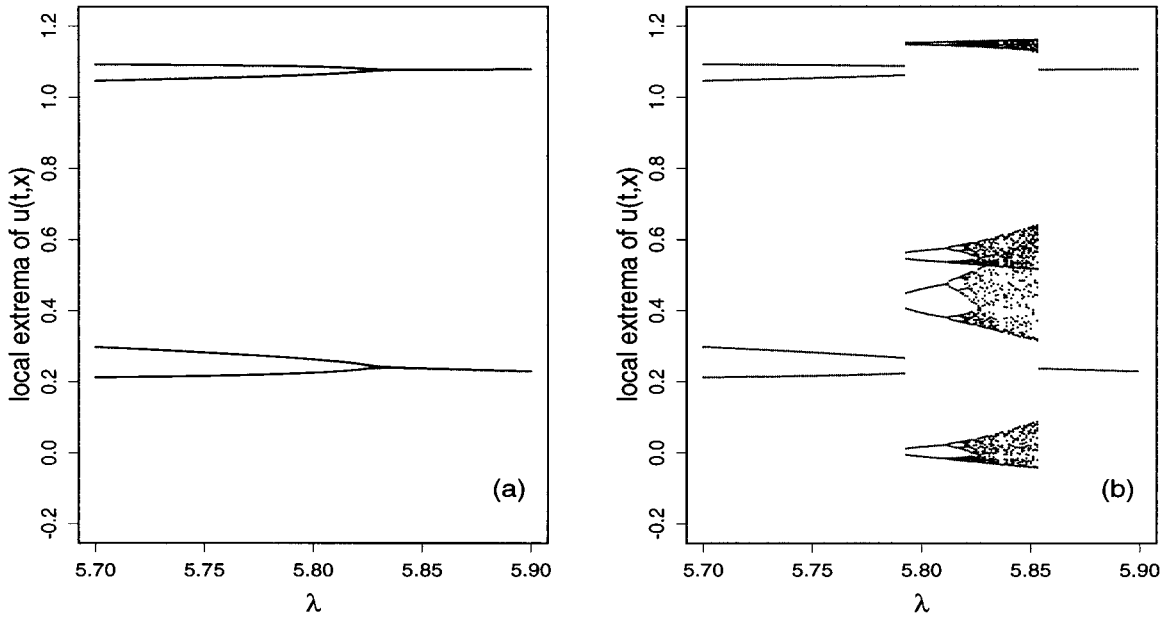

FIG. 6. (a) Solution bifurcation behaviour along the x characteristics using the solution at $\lambda = 5.79$ as an initial condition. (b) Magnification of the bifurcation diagram in Figure 4 for $5.79 < \lambda < 5.89$.

solution at λ) give rise to solutions which converge to attractor B as $t \to \infty$. If the initial condition is given by the solution for a value of λ such that $5.79265 < \lambda < 5.85408$, then the solution converges to attractor B as $t \to \infty$. If the initial condition is given by a solution for $\lambda = 5.79265$ or $\lambda = 5.85408$ then the solution converges to attractor A as $t \to \infty$. Thus $\lambda = 5.85408$ and $\lambda = 5.79265$ are on the boundary of the basin of attraction. In Figure 8 the solution bifurcation behaviors are shown for $5.7315 < \lambda < 5.7319$ with the initial condition taken as the solution at $\lambda = 5.792654$. The solution is plotted for $500 < t < 600$ and the λ's are incremented by 10^{-7}. This figure shows what happens when one attractor is replaced by another attractor.

Due to the appearance of a new cycle of period 4 and to the rounding at the extremities of the branches at the beginning of the new cycle of period 4 in Figure 7a and Figure 8, we are led to conjecture that at the value of λ corresponding

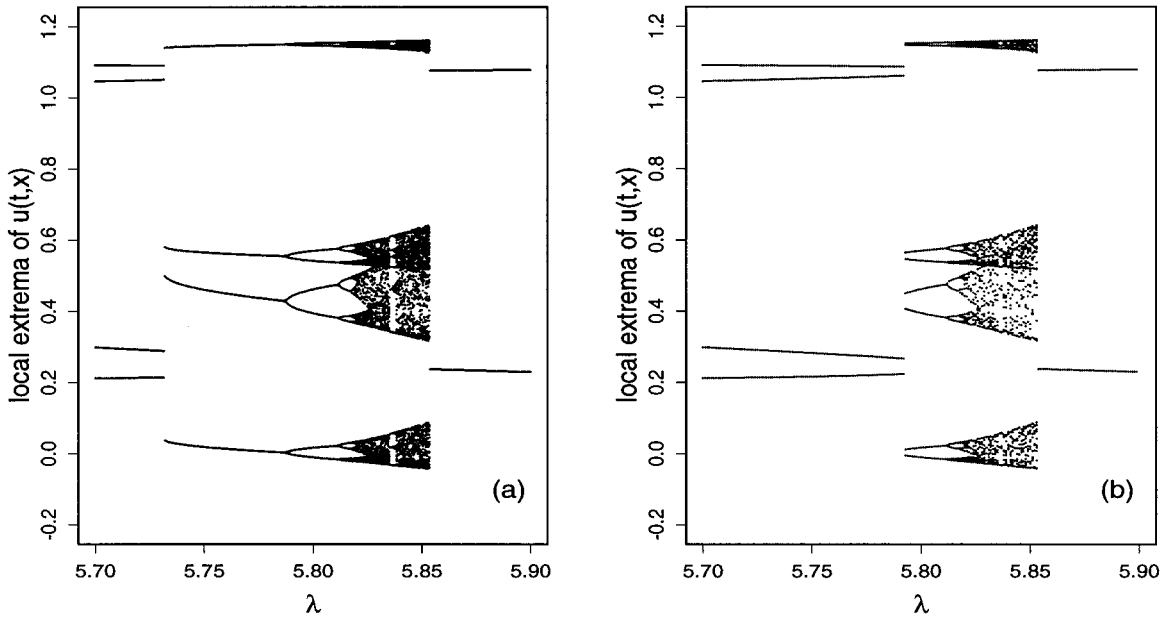

FIG. 7. (a) Solution bifurcations along the x characteristics using the solution at $\lambda = 5.81$ as an initial condition. (b) Magnification of the bifurcation diagram in Figure 4 for $5.79 < \lambda < 5.89$.

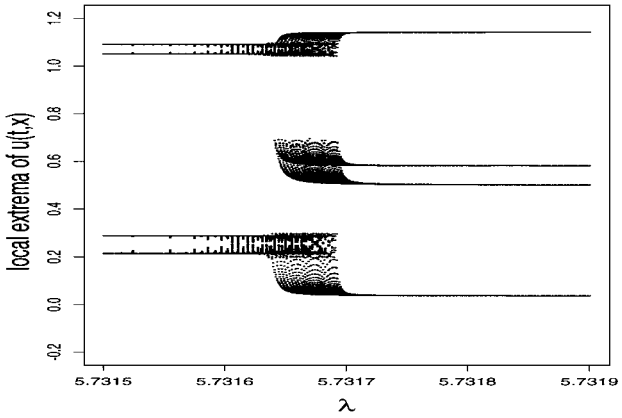

FIG. 8. Solution behaviour when attractor A is replaced by attractor B.

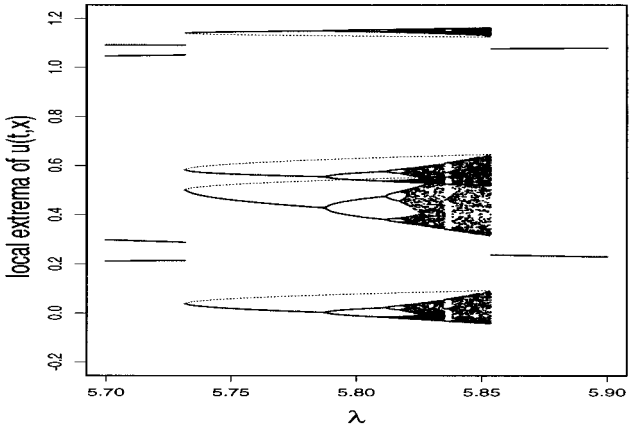

FIG. 9. Potential unstable cycle of period 4.

to the lower limit of the basin of attraction ($\lambda \simeq 5.79265$), at which the new cycle of period 4 appears, a tangent bifurcation occurs creating a stable and unstable cycle of period 4.

We further conjecture that at the value of λ corresponding to the upper limit of the basin of attraction ($\lambda \simeq 5.85408$) the unstable cycle of period 4 collides with the chaotic attractor causing the destruction of the chaotic attractor. This would agree with the Grebogi *et al.* conjecture.[42] Figure 9 shows the postulated unstable cycle of period 4 (plotted as dashed curves).

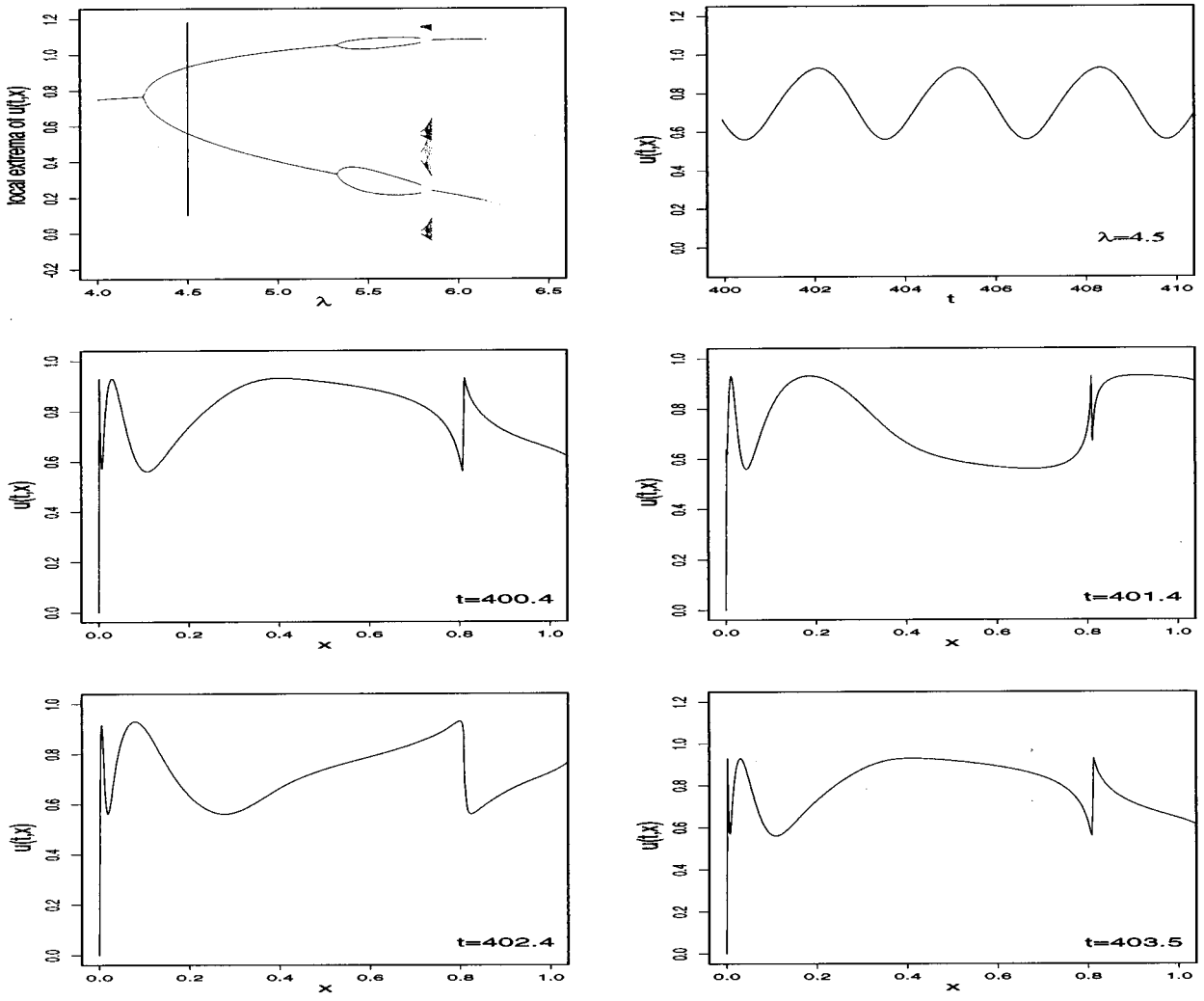

FIG. 10. Temporal and spatial solution for $\lambda = 4.5$.

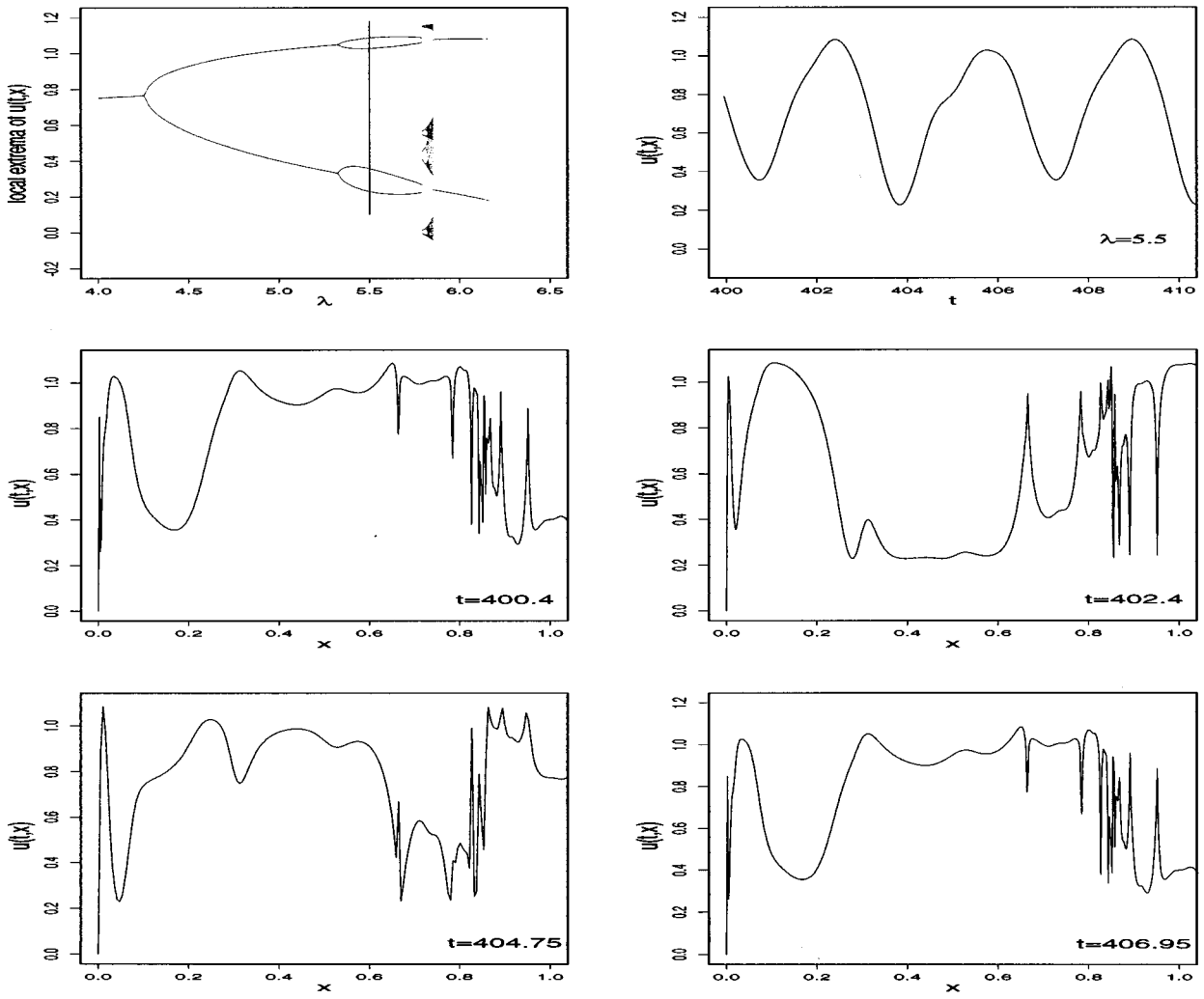

FIG. 11. Temporal and spatial solution for $\lambda = 5.5$.

3. Spatial solution behaviour occurring after the Hopf bifurcation

In Figures 10–13 the solution is shown as a function of x [remember that x is the maturation variable of the model equation (19)]. In the top left hand corner of each of these figures the temporal bifurcation diagram is shown. In the top right hand corner the solution is shown as a function of t along the x characteristics. The four other plots are solutions as functions of the maturation variable.

As in the previous section, these solutions were obtained using the method of characteristics. δ and r were held constant at the values $\delta = 1$ and $r = 0.0001$. Each solution was calculated for a given t on 700 characteristics equally spaced on the interval [0,1].

In Figure 10 the solutions are shown for $\lambda = 4.5$. Since $r << 0.7455$, the spatial and temporal Hopf bifurcation occur simultaneously. Thus in both cases the solution is just above the Hopf bifurcation. The length of the temporal period is approximately 3.1. The spatial solutions shown span the whole length of the temporal period and thus the solution at $t = 400.4$ appears identical to the solution at $t = 403.5$. As shown in Ref. 4, if we denote the period in the (t,x) plane by T_x and the period along the characteristics by T_c, then near the Hopf bifurcation we have $T_x = T_c/(1-r)$, in agreement with these observations.

This behaviour is again mirrored in Figure 11 where the solutions are shown for $\lambda = 5.5$. The temporal solution has undergone a period doubling and the length of the period is approximately 6.55. The spatial solutions shown again span the length of the period and the solution at $t = 400.4$ is almost identical to the solution at $t = 406.95$ in spite of the fact that the first period doubling has taken place.

Comparing Figure 11 to Figure 10, note that the amplitude of the spatial solution has increased and the solution has become more structured.

In Figure 12 the solutions are shown for $\lambda = 5.8$. The temporal solution has undergone a secondary bifurcation from a cycle of period 4 to a cycle of period 8. The length of the period is now approximately 8.2. The spatial solutions shown again span the whole length of the period; however this time, as one can see by comparing the plots for $t = 400.4$ and $t = 408.6$ in Figure 12, the solution at

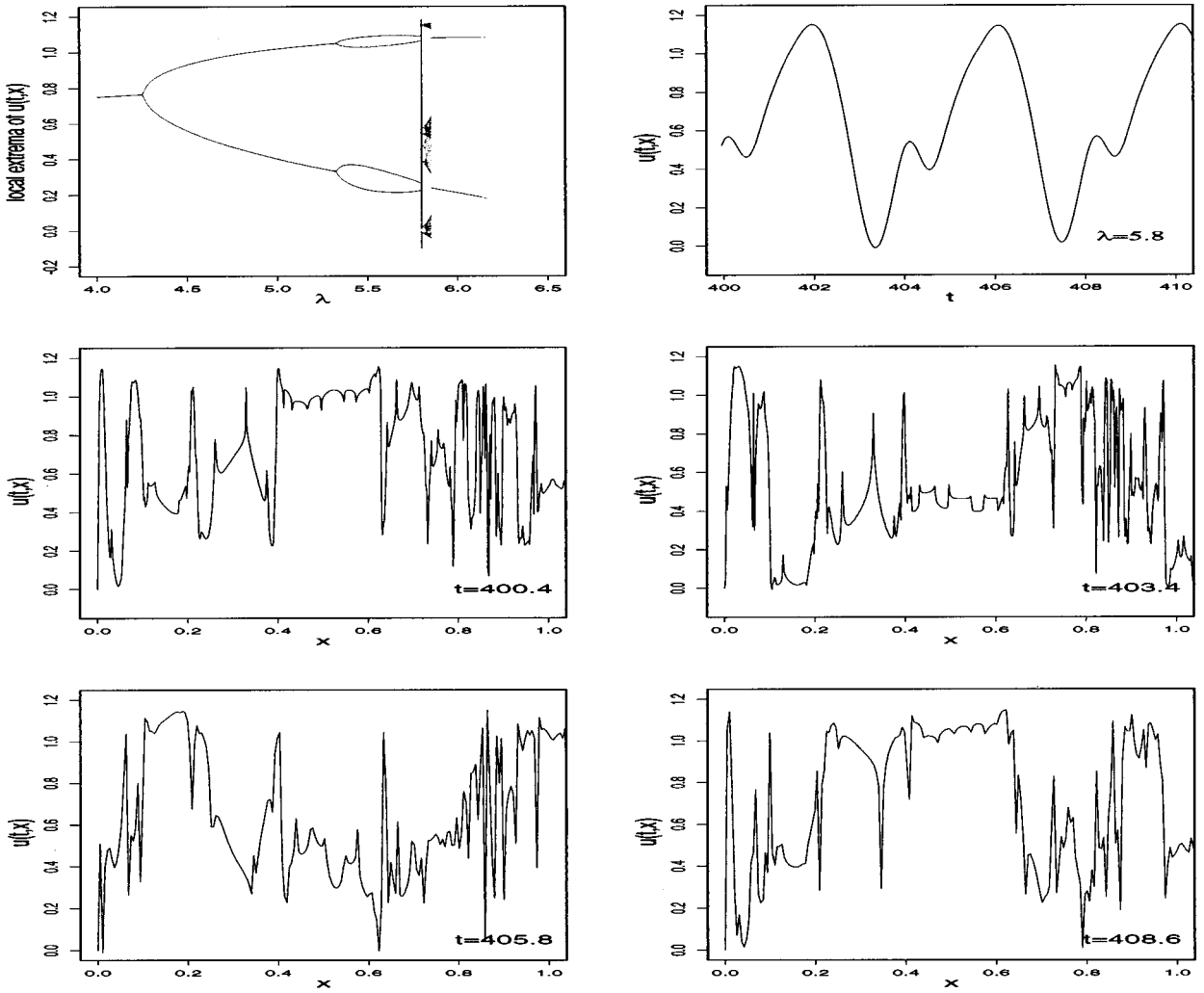

FIG. 12. Temporal and spatial solution for $\lambda = 5.8$.

$t = 400.4$ is not identical to the solution at $t = 408.6$ (this discrepancy in solutions is not improved by increasing the precision of the length of the period). This discrepancy is not unexpected considering the fact that for this case λ is much further from the Hopf bifurcation point.

Comparing Figure 12 to Figure 11 shows that the spatial solution has become even more structured. In Figure 13 the solutions are shown for $\lambda = 6$. The temporal solution has undergone a reverse bifurcation and is again a cycle of period 2. The length of the period is approximately 3.35. The spatial solutions shown span the length of the period and the solution at $t = 400.4$ is almost identical to the solution at $t = 403.75$ (note that for $\lambda = 6$, attractor A has regained its stability). The spatial solution has become extremely structured.

Clearly, increasing the parameter λ causes the maturational dependence of the solution to become progressively more structured. The increase in structure in the solution as a parameter is varied and has been studied extensively by Sharkovsky *et al.*[53] for *functional* iteration under the action of a map,

$$f(t+1) = \mathscr{S}(f(t)), \quad t \in \Re^+, \tag{50}$$

where $\mathscr{S}: I \to I$ is a given function, $I \in \Re^1$ is a closed, bounded interval, and $f(t) \in \Re^+$ is an unknown function. They investigated how the structure of the solution for large iteration numbers depends on the relationship between the map $\mathscr{S}$ and the identity line, and showed how very ''turbulent'' solutions may arise in some circumstances. Noting that from (26) along the characteristics we may write

$$u(t+\tau, x_0 e^{-r(t+\tau)}) = e^{-\delta t}\left\{ u(\tau, x_0 e^{r\tau}) + \lambda \int_0^t e^{\delta z} \mathscr{F}(u(z, x_0 e^{rz}))\, dz \right\}; \tag{51}$$

in some qualitative sense the same phenomena must be occurring for the system studied here.

An interesting feature in the spatial plots in Figure 10 is the sharp reversal of slope at approximately $x = 0.8$. To ex-

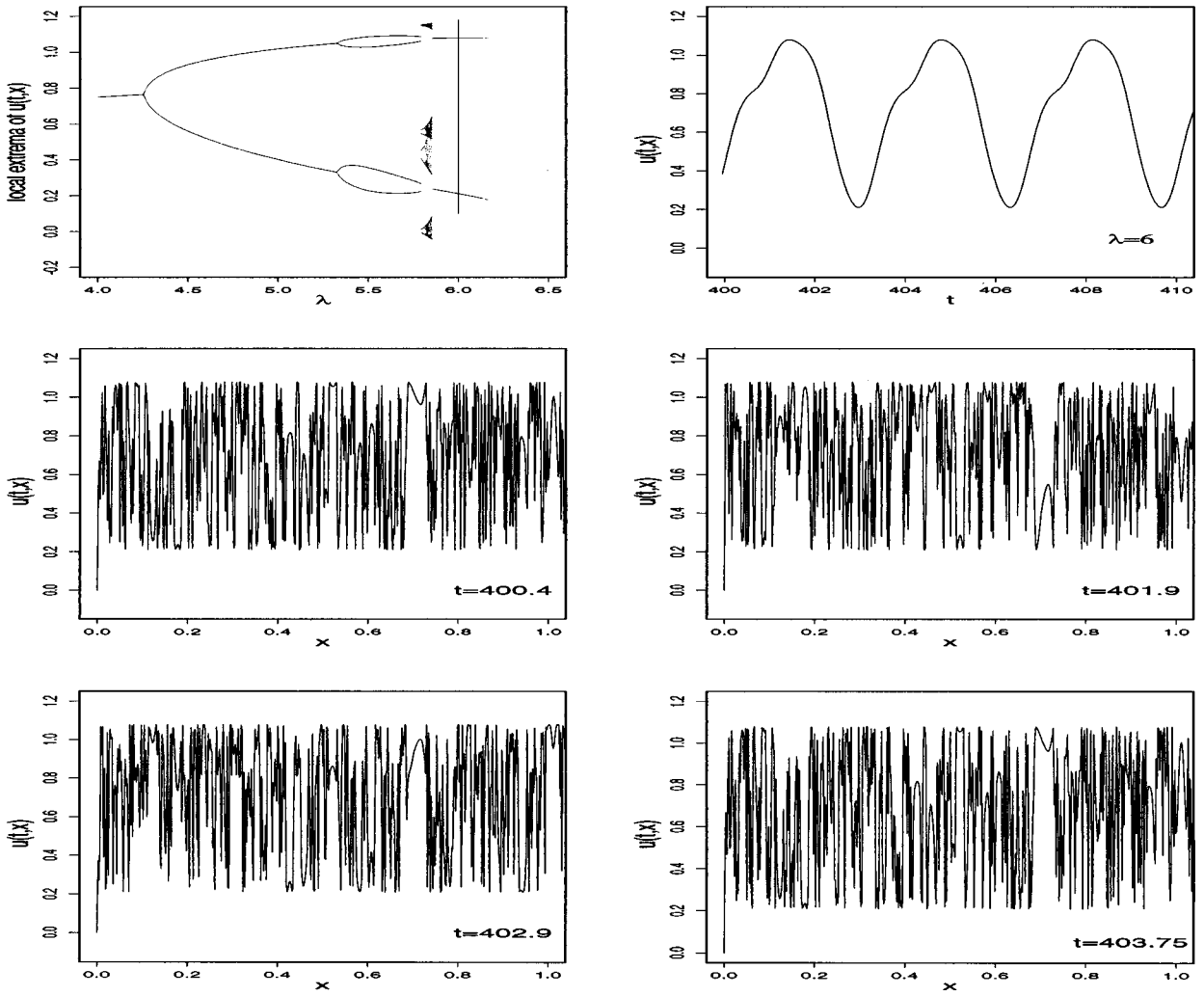

FIG. 13. Temporal and spatial solution for $\lambda=6$.

plore this further, in Figure 14 the spatial solution for various values of λ is plotted. Each plot shows the solution for ten times (the times are incremented by 0.1). The plot for $\lambda=4.2$ in Figure 14 shows the solution just above the Hopf bifurcation. The amplitude of the solution very close to the Hopf bifurcation is small. With magnification of Figure 14 (not shown) one can see that the solution has a node at $x\simeq 0.77$ which corresponds to $u(t,x)=0.7619$. The value of $u(t,x)$ at this node is the value of the steady state $(\lambda-\delta)/\lambda$ for $\lambda=4.2$ and $\delta=1$. Thus the node is created when the solution for various times simultaneously attain the value of the steady state $(\lambda-\delta)/\lambda$. As λ is slowly increased and the solution moves away from the Hopf bifurcation the node becomes a line which lengthens as the amplitude of the solution increases. This is illustrated in Figure 14. Further work is needed to explain this phenomenon.

C. Section summary

The nonlinear partial differential delay equation,

$$\frac{\partial u}{\partial t}+rx\frac{\partial u}{\partial x}=-\delta u+\lambda u_{\tau}(1-u_{\tau}), \tag{52}$$

where $u_{\tau}(t,x)\equiv u(t-\tau,xe^{-r\tau})$, has an extremely rich array of solution behaviour.

As λ, the maximal proliferation rate, is varied the temporal solution undergoes a period doubling route to chaos. The chaotic band thus obtained contains periodic windows whose behaviour can be explained by the presence of crises. It was also shown that the temporal solution has two coexisting attractors and hence is multistable.

The spatial solution becomes more structured as λ is increased and at $\lambda=6$ is extremely turbulent. The spatial solution displays two interesting phenomena.

(1) The further one is away from the Hopf bifurcation line, the greater the discrepancy between the period T_c along the characteristics and the period T_x in the (t,x) plane (e.g., the spatial solution at $\lambda=5.8$ does not repeat itself after one period T_c).
(2) There is a node at the steady state $(\lambda-\delta)/\delta$ for spatial solutions just past the Hopf bifurcation. As the solution moves further away from the Hopf bifurcation, the node becomes a static front.

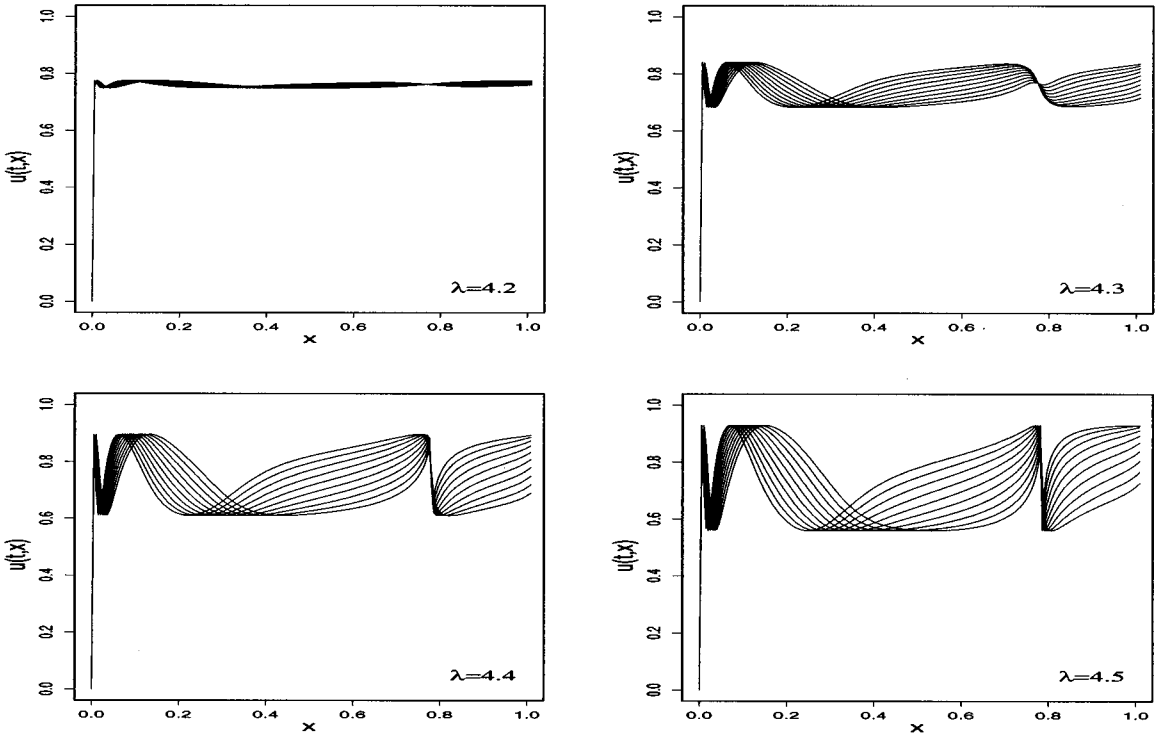

FIG. 14. Spatial solutions just above the Hopf bifurcations for four values of λ and ten times.

Further work is needed in order to fully understand both of these phenomena.

Though this behaviour is interesting in its own right, it has further potentially interesting biological implications since the process of cell population replenishment via bone marrow transplant may be viewed as the imposition of a different initial function on the cell replication dynamics. Our simulation results indicate that, depending on the maximal proliferation rate, the resulting dynamics may differ dramatically from trial to trial depending on the precise form of the initial function. Extrapolating this into the bone marrow transplant situation, they would indicate that small changes in the maturity composition of the transplanted cells could lead to dramatically different dynamic patterns of transplant engraftment.[55–57] This problem has been considered by Schwegler and Mackey[11] from quite a different modeling perspective.

VI. DISCUSSION AND SUMMARY

Numerical solutions to a model equation that describes cell population dynamics have been presented and analyzed. A distinct feature of the model equation is the presence of delayed arguments in the time and maturation variables due to the nonzero length of the cell cycle. This transport-like equation balances a linear convection $r(\partial u/\partial x)$ with a nonlinear reaction term $[-\delta u+\lambda u_\tau(1-u_\tau)]$, where $u_\tau(t,x)=u(t-\tau,x\ \exp(-r\tau))$. The linear convection term $r(\partial u/\partial x)$ acts to impress the value of $u(t,x=0)$ on the entire population while the death term $(-\delta u)$ acts to drive the population to extinction $(u=0)$. The rich phenomenology of solution behaviour presented here arises from the nonlinear, nonlocal birth term $(\lambda u_\tau(1-u_\tau))$. The existence of this kinetic nonlinearity accounts for the existence and propagation of soliton-like or front solutions, while the increasing effect of nonlocality and temporal delays acts to produce a fine periodic structure on the trailing part of the front. This nonlinear, nonlocal, and delayed kinetic term is also shown to be responsible for the existence of a Hopf bifurcation and subsequent period doublings to apparent ''chaos'' along the characteristics of this hyperbolic partial differential equation. In the time maturation plane, the combined effects of nonlinearity, nonlocality, and delays leads to solution behaviour exhibiting spatial chaos for certain parameter values.

Although analytic results are not available for the system we have studied, consistency and validation of the numerical results was achieved by using different numerical methods. A general conclusion of this work, of interest for the understanding of any system modeled by a hyperbolic delayed partial differential equation, is that increasing the spatiotemporal delays will often lead to spatial complexity and irregular wave propagation.

ACKNOWLEDGMENTS

We would like to thank Professor J. A. Yorke for his comments on the results of Section V, and the Faculty of Graduate Studies and Research of McGill University for a grant to defray the computational costs of this research, and for support to RC. MCM and AR also thank the Natural Sciences and Engineering Research Council (NSERC) of Canada for support through operating grants, while MCM

thanks the Alexander von Humboldt Stiftung and the Royal Society of London for generous research support.

[1] J. A. J. Metz and O. Diekmann, in *The Dynamics of Physiologically Structured Populations* (Springer-Verlag, New York, 1986).
[2] M. C. Mackey and J. G. Milton, Commun. Theor. Biol. **1**, 299 (1990).
[3] M. C. Mackey and R. Rudnicki, J. Math. Biol. **33**, 89 (1994).
[4] A. D. Rey and M. C. Mackey, Can. Appl. Math. Qu. **1**, 61 (1993).
[5] A. D. Rey and M. C. Mackey, Chaos **2**, 231 (1993).
[6] A. D. Rey and M. C. Mackey, Physica D **80**, 120 (1995).
[7] A. D. Rey and M. C. Mackey, Physica D **86**, 373 (1995).
[8] M. C. Mackey, Blood **51**, 941 (1978).
[9] W. P. Hammond, T. C. Boone, R. E. Donahue, L. M. Souza, and D. C. Dale, Blood **76**, 523 (1990).
[10] A. R. Migliaccio, G. Migliaccio, D. C. Dale, and W. P. Hammond, Blood **75**, 1951 (1990).
[11] M. C. Mackey and H. Schwegler, J. Stat. Phys. **70**, 281 (1993).
[12] H. Schwegler and M. C. Mackey, J. Math. Biol. **32**, 761 (1994).
[13] A. Lasota, Nonlin. Anal. **5**, 1181 (1981).
[14] B. Alberts, D. Bray, J. Lewis, M. Raff, K. Roberts, and J. Watson, *Molecular Biology of the Cell* (Garland, New York, 1983).
[15] K. L. Cooke and Z. Grossman, J. Math. Anal. Appl. **86**, 592 (1982).
[16] S. P. Blythe, R. M. Nisbet, and W. S. C. Gurney, Theor. Pop. Biol. **25**, 289 (1984).
[17] S. P. Blythe, R. M. Nisbet, W. S. C. Gurney, and N. MacDonald, J. Math. Anal. Appl. **109**, 388 (1985).
[18] N. Macdonald, *Biological Delay Systems: Linear Stability Theory* (Cambridge University Press, Cambridge, 1989).
[19] R. F. V. Anderson, Math. Biosci. **105**, 81 (1991).
[20] R. F. V. Anderson, J. Math. Anal. Appl. **163**, 184 (1992).
[21] R. F. V. Anderson, J. Dyn. Diff. Eqn. **5**, 105 (1993).
[22] M. C. Mackey and P. Dörmer, Cell Tissue Kinet. **15**, 381 (1982).
[23] C. S. Potten and M. Loeffler, Development **110**, 1001 (1990).
[24] G. C. Nooney, Biophys. J. **7**, 69 (1967).
[25] D. G. Oldfield, Bull. Math. Biophy. **28**, 545 (1966)
[26] H. von Foerster, *The Kinetics of Cellular Proliferation*, edited by F. Stohlman (Grune and Stratton, New York, 1959).
[27] S. I. Rubinow, Biophys. J. **8**, 1055 (1968).
[28] E. Zauderer, *Partial Differential Equations of Applied Mathematics* (Wiley, New York, 1983).
[29] C. A. J. Fletcher, *Computational Galerkin Methods*, Springer Series in Computational Physics (Springer-Verlag, New York, 1984).
[30] E. Becker, G. F. Carey, and J. Tinsley Oden, *Finite Elements: An Introduction* (Prentice–Hall, Englewood Cliffs, NJ, 1981).
[31] L. Lapidus and G. F. Pinder, *Numerical Solution of Partial Differential Equations in Science and Engineering* (Wiley, New York, 1982).
[32] P. Brunovský, Nonlin. Anal. **7**, 167 (1983).
[33] P. Brunovský and J. Komorník, J. Math. Anal. Appl. **104**, 235 (1984).
[34] A. Lasota, K. Loskot, and M. C. Mackey, Acta Biotheor. **39**, 1 (1991).
[35] K. Loskot, J. Diff. Eqn. **58**, 1 (1985).
[36] R. Rudnicki, Erg. Theor. Dynam. Sys. **5**, 437 (1985).
[37] R. Rudnicki, Bull. Pol. Acad. Sci. Math. **35**, 289 (1987).
[38] R. Rudnicki, J. Math. Anal. Appl. **132**, 14 (1988).
[39] P. Collet and J-P. Eckmann, Nonlinearity **6**, 1265 (1992).
[40] V. I. Karpman, *Non-linear Waves in Dispersive Media* (Pergamon, Oxford, 1975).
[41] J. Hale, *Theory of Functional Differential Equations* (Springer-Verlag, New York, 1977).
[42] C. Grebogi, E. Ott, and J. Yorke, Physica D **7**, 181 (1983).
[43] P. Battelino, C. Grebogi, E. Ott, and J. Yorke, Physica D **32**, 296 (1988).
[44] S. McDonald, C. Grebogi, E. Ott, and J. Yorke, Phys. Lett. A **107**, 51 (1985).
[45] C. Grebogi, E. Ott, and J. Yorke, Science **238**, 632 (1987).
[46] J. M. Aguirregabiria and J. R. Etxebarria, Phys. Lett. A **122**, 241 (1987).
[47] R. Crabb, J. Losson, and M. Mackey, Proc. First World Cong. Nonlin. Anal. **4**, 3125 (1996).
[48] K. Ikeda, Appl. Phys. B **28**, 257 (1979).
[49] K. Ikeda and K. Matsumoto, Physica D **29**, 223 (1987).
[50] K. Ikeda, K. Kondo, and O. Akimoto, Phys. Rev. Lett. **49**, 1467 (1982).
[51] J.-N Li and B.-L. Hao, Commun. Theor. Phys. **11**, 265 (1989).
[52] J. Losson, M. Mackey, and A. Longtin, Chaos **3**, 1 (1993).
[53] A. Sharkovsky, Yu Maistrenko, and E. Romanenko, *Difference Equations and Their Applications* (Kluwer Academic, New York, 1993).
[54] R. Vallée and C. Delisle, Phys. Rev. A **34**, 309 (1986).
[55] L. Glass and M. C. Mackey, *From Clocks to Chaos* (Princeton University Press, Princeton, NJ, 1988).
[56] A. Lasota, M. C. Mackey, and M. Wazewska-Czyzewksa, J. Math. Bio. **19**, 43 (1981).
[57] J. G. Milton and M. C. Mackey, J. R. Colloq. Phys. London **23**, 236 (1989).